AD-A097 034   NAVAL RESEARCH LAB WASHINGTON DC   F/G 11/6
              FATIGUE CRACK GROWTH IN A36/A283 PLATE IN AIR AND SEA WATER ENV--ETC(U)
              MAR 81   F R STONESIFER, J M KRAFFT
UNCLASSIFIED NRL-MR-4467   NL

END
DATE
FILMED
4-81
DTIC

REPORT DOCUMENTATION PAGE

READ INSTRUCTIONS
BEFORE COMPLETING FORM

1. REPORT NUMBER	2. GOVT ACCESSION NO.	3. RECIPIENT'S CATALOG NUMBER
NRL Memorandum Report 4467	AD-A097034	

4. TITLE (and Subtitle)	5. TYPE OF REPORT & PERIOD COVERED
FATIGUE CRACK GROWTH IN A36/A283 PLATE IN AIR AND SEA WATER ENVIRONMENTS	Interim report on continuing NRL Problem
	6. PERFORMING ORG. REPORT NUMBER

7. AUTHOR(s)	8. CONTRACT OR GRANT NUMBER(s)
F. R. Stonesifer and J. M. Krafft	

9. PERFORMING ORGANIZATION NAME AND ADDRESS	10. PROGRAM ELEMENT, PROJECT, TASK AREA & WORK UNIT NUMBERS
Naval Research Laboratory Washington, D.C. 20375	58-0263-0-1; RR023-03-45

11. CONTROLLING OFFICE NAME AND ADDRESS	12. REPORT DATE
Naval Research Laboratory Washington, D.C. 20375	March 26, 1981
	13. NUMBER OF PAGES
	32

14. MONITORING AGENCY NAME & ADDRESS(if different from Controlling Office)	15. SECURITY CLASS. (of this report)
	Unclassified
	15a. DECLASSIFICATION/DOWNGRADING SCHEDULE

16. DISTRIBUTION STATEMENT (of this Report)

Approved for public release; distribution unlimited.

17. DISTRIBUTION STATEMENT (of the abstract entered in Block 20, if different from Report)

18. SUPPLEMENTARY NOTES

19. KEY WORDS (Continue on reverse side if necessary and identify by block number)

Fatigue Crack Propagation
Structural Steel/Fatigue
Corrosion Fatigue

20. ABSTRACT (Continue on reverse side if necessary and identify by block number)

Extensive use of A36 type steels in wave-excited marine structures raises the question of its resistance to fatigue crack propagation in the sea water environment. Above its ductile-brittle transition temperature, static fracture of such a low strength steel usually entails extensive plastic deformation. However with cyclic loading, fatigue cracks can grow with little plastic flow, at crack loading levels well below that required for fracture instability. The hazard entailed has the positive benefit of allowing linear elastic fracture mechanics to be utilized in applying test data to problems of structural life prediction. To this end, this paper reports crack growth data on A36 plate at laboratory temperature in air

(Continued)

DD FORM 1473 EDITION OF 1 NOV 65 IS OBSOLETE
1 JAN 73
S/N 0102-LF-014-6601

i

20. ABSTRACT (Continued)

and in synthetic sea water. Two extremes of mean stress or stress ratio R = 0 and 0.8 typify the ordinary condition as well as growth in the residual stress field of a constrained weld. Varied cyclic frequencies as low as 0.1 Hz reach as low as the natural sway frequencies of very large structures at sea. The new data is compared with literature data from other structural steels using fitting parameters of the NRL tensile ligament instability model for crack propagation. Results indicate that no relief from corrosion fatigue effects is derived from the relatively low yield strength level of this steel.

CONTENTS

iii

FATIGUE CRACK GROWTH IN A36/A283 PLATE IN AIR AND SEA WATER ENVIRONMENTS

I. INTRODUCTION

Prior to the 1975 reports of Vosikovsky [1], there had been little concern for sea water environmental effects on fatigue crack growth in mild steels. Earlier work of Brown and Sandoz [2] had shown a K-threshold for stress corrosion cracking comparable to the measurable fracture toughness for steels of yield strength as high as 1000 MPa (150 ksi). But with cyclic loading, Vosikovsky's X65 line-pipe steel exhibited substantial crack growth acceleration in salt water at applied ΔK levels far below crical fracture toughness. Applied cathodic protection increased the growth rate even more. In 1975, Scott and Sylvester [3] reported marked effects of North Sea water on BS4360 Grade 50D plate, and in 1977 even larger effects at elevated mean stress, or stress ratio. More recently Bamford [4] has shown accelerated crack growth for pressure vessel steels in an environment simulating a pressurized water nuclear power reactor.

The effect of such crack growth rate increases on fatigue design allowables depends on the extent of structural life prior to crack initiation. Considering welds as the most likely crack sources, Lawrence [5] shows the initiation portion of total endurance to become rather small at low strength levels in steels. Indeed from extensive work on structural steel weldments, Gurney [6] suggests the complete neglect of an initiation period and that only the crack propagation life, from inevitable indigenous defects, should be used to estimate fatigue life. With good reason then, there is concern that current weld design criteria may prove nonconservative for conditions of wave loading with sea water immersion.

A rather large international research effort is currently devoted to resolving these questions. This paper reports a program at the Naval Research Laboratory, investigating the structural steel most commonly used in the United States, A36/A283 Grade C. It is of necessity a limited result; fatigue testing is inherently tedious and time consuming. Placed in context with the existant body of literature data, it is hoped that it will provide a useful supplement by extending the data base to include a material of very low yield strength level.

The crack propagation tests w··· performed in general conformity with ASTM Test Method #647-78T [7]. However, since our program was planned and specimens procured before the standard was issued, some deviations persisted. Thus a standard 1-T compact tension specimen, with width W = 51 mm was employed. In order to obtain maximum transverse restraint or degree of plane strain, the full plate thickness of 25 mm was used. This is at the extreme upper limit permitted by the ASTM Test Method. Use of the compliance method for crack length determination obviated the need for crack curvature correction. In general, fracture surface markings on broken specimen halves indicated acceptable degrees of crack straightness despite the extra thickness. Typically, measurements ranged from starting precracks of near 0.3W to fracture instability at about 0.65W. With a (lower) yield strength of about 260 MPa, this specimen meets the size requirements, when $a = \frac{W}{2}$, up to $K_{max} \cong 26$ MPa $\sqrt{in.}$ Actually, the point at which crack growth becomes unstably fast, associated with ligament yielding, is about $K_{max} = 45$ MPa $\sqrt{in.}$ Results shown for K_{max} levels in the range 26 to 45 MPa $\sqrt{in.}$ should be regarded provisionally.

Our procedure differs from that of ASTM Method 647 in that crack growth was estimated from load vs notch opening compliance slopes rather than surface-crack traces. Validated by work of Sullivan and Crooker [8], this indirect method allows crack length determination without removing specimens from the liquid chamber. Compliance vs crack length was calibrated on specimens of the same plate material using fatigue cracks marked by cycling blocks of reduced stress amplitude to provide visible "beach marks". We have not determined the absolute precision of this method but believe it to meet the requirements of ASTM E647, Sec. 8.6.

2

The specimens were loaded in an electro-hydraulic servo-controlled testing system assembled at NRL from components manufactured by several companies. A 20 gallon per minute (gpm) pump supplied hydraulic oil at 3,000 psi pressure to an 11 KIP actuator through a 5 gpm servo valve. The actuator and an 11 KIP load cell were mounted in a frame rated at 100 KIP. The electronics were calibrated to read in the metric system with the maximum of 5 load ranges at 5,000 Kg (11 KIP). The loading frame was placed with the load axis horizontal to the floor. This position allowed the crack beyond the loading pins to be immersed in the sea water.

The A36 steel plate for the test program was purchased from a warehouse in Baltimore and was not pedigreed. A 2.54m × 0.457m plate, 25 mm thick was obtained. Chemical analysis #97732 by Ledoux and Company showed it to fall within the limits of ASTM specifications for A283 Grade C: C 0.17%, Mn 0.86, P 0.015, S 0.021, Si 0.29, Cu 0.03, O 0.065, H 0.0005. We are unaware of any heat treatment following its rolling. Standard 0.505 in. (12.83 mm) diameter tensile specimens, and Charpy V-notch specimens were prepared and tested. The 30 degree C tensile properties are within specification: lower yield strength 256 MPa, ultimate tensile stress 465 MPa, reduction in area at rupture 59%, and elongation in 2 in. gage length 30%.

A Charpy energy of 24J was found at -15 degrees C, with 20J (15 ft lb) at -20 degrees C. Specimens were oriented to provide cracks of long transverse TL orientation.

Specimens were fatigue pre-cracked from a milled 60 degree notch in general conformance with Sec. 8.3 of Method E-647.

A sinusoidal cyclic loading wave was employed in precracking as well as in fatigue testing. The loading variables are: stress ratio- 0 and 0.8; cyclic frequency- 0.1, 1, 3, and 10 Hz. It was necessary to briefly reduce the two highest frequencies by 1/10, during each compliance measurement to ensure recording accuracy. Since this is merely a frequency excursion, and not one of load, it should not have affected the data. Maximum load levels ranged from 1361 to 4536 kg to cover the required levels of ΔK.

Two environmental conditions were compared: ambient air and simulated sea water. The laboratory is air-conditioned to a temperature of 24 plus or minus 3 degrees C. Humidity was not controlled, but its variation is believed to have no effect on the growth rate for mild steel. The brine was formulated by mixing a commercial (special) sea salt with local tap water in proportions of 1 premeasured packet to 5 gallons as recommended by the manufacturer. A neutral pH was estimated. Absorbed oxygen content was not measured. The brine was gravity fed to drip onto the notch at a rate of about 600ml/hr, thence collected in a receptacle containing the lower portion of the specimen. Overflow at the brim of the primary trough was collected in another pan and pumped back to the reservoir, a large Nalgene plastic bottle. All parts of the system except specimen, grips, and rods were of inert plastic. After rust had excessively stained the brine, it was replaced with fresh solution.

The modeling procedure used to compare the new fatigue crack growth (FCG) data with sets for other steels requires full monotonic and cyclic stress-strain curves of each steel. This is done with specimens small enough to be excised from a broken half of the standard 1T-CT specimens which were used for the crack growth rate measurements. An overall length of 38 mm contains 12.7 mm threaded buttons to either end of a cylindrical gage section 4.3 mm in diameter and about 2 diameters in length between fillets. It was cycled in an alignment subpress adapted to the lower headspace of a 45 kN screw-driven Instron testing machine. A longitudinal strain gage was employed with a conventional X-Y recorder to display the stress-strain curves. A stress relaxation, run at elevated stress sensitivity, provided data for the stress relaxation exponent m, needed in the modeling equations.

II. CRACK-GROWTH-RATE DATA PROCESSING

Data processing leading to growth rate plots both manual and computerized processes, involved two steps. The load vs notch-opening records were manually scaled for slope. After normalization for any variation from the nominal one inch (25.4 mm) thickness, crack length was estimated from the compliance calibration curve. The resulting crack length, a, was plotted vs cumulative cycles, N, on an appropriate scale. Determinations of crack growth rate from the slope of a curve fitted to each a vs N plot gave a reasonable smoothing through the scatter of points obtained by calculating slopes between

4

adjacent measurement points. This step served to screen the data for gross inconsistencies and to provide a check on later computer processing of the data.

The computer processing employed the automatic data-processing facility developed at NRL by Cullen et al [9]. Since our density of data points, manually collected, was low compared to that of Cullen's automatic sampling, a compromise to the ASTM recommended seven-point incremental polynomial method was used. A second-order polynomial method was fitted to each successive set of five data points. A fit to only three points left too much scatter; the seven-point technique suggested in ASTM Test #647, provided no significant additional smoothing. In the Cullen algorithm, forward and backward regression is used at the ends of each data set to afford differentiability up to the first and last points of the data set. The X-Y plotter of this system was programmed to provide a log-log scale which matched a standard graph paper, CODEX 31119.

III. CRACK GROWTH RATE DATA

Results of the computer data processing and plotting are first shown for each individual test condition, Figs. 1-11; then grouped with respect to stress ratio, Figs. 12 and 13. The captions and legends on each figure identify its test conditions, which, as noted earlier, comprise cyclic frequencies from 10 to 0.1 Hz, stress ratios of zero and 0.8, and environments of room temperature air and synthetic sea water.

The composite plot of all data at stress ratio $R = 0$, Fig. 12, presents an unexpected result. Crack growth rates in air at all cyclic frequencies and in salt water at frequencies greater than 1.0 Hz all occupy the same scatter band. On the other hand, cyclic growth rates at lower frequencies, 0.3 and 0.1 Hz, are considerably accelerated by sea water; the data indicates at least a three fold increase. The coincidence of data points for both the low frequencies suggests an absecne of a frequency dependency, as would be expected for stage one growth. The unexpected trend is the absence of any discernable frequency-dependent stage two. It is as though at a frequency of 1.0 Hz, or cycle period of one second, the stage-two transition is at a crack growth rate less than 3×10^{-5} mm/cycle. But with a cycle period

of 3 seconds or longer, it is at a level more than 10 times as rapid. We are aware that there is some precendent for an indistinct second stage. Work of Sullivan and Crooker on A516-60 structural steel [10] showed a similar absence of stage two growth in fast flowing sea water, both freely corroding and with cathodic protection. However, in a still solution, the zinc-coupled specimen showed an accelerated stage one growth followed by a distinct, ΔK-independent, presumably frequency dependent, stage two. Scott and Sylvester [3], show the stage two transition to be rather narrow, hence difficult to discern in the freely corroding condition but accentuated by imposed potential. The stage two transition at 0.1 Hz typically occurs at crack growth rates in the range of one micron per cycle, with ΔK levels of about 30 MPa $\sqrt{in.}$ At this ΔK level a steel as soft as A-36, with the present 1-T specimen size, could suffer crack acceleration due to an excessive cyclic plastic zone size, which then could mask observation of the stage-two transition. Whatever the reason, a stage two transition is difficult to discern in the present data set.

For data at high stress ratio $(R = 0.8)$, Fig. 13, only the threshold region is free of general yielding. Thus if crack growth acceleration due to general yielding occurs at $\Delta K = K_{max} = 45$ for $R = 0$, it occurs for $\Delta K = 9$ for $R = 0.8$. As to threshold behaviors, present data is in itself not conclusive. At the high stress ratios, the threshold region was probed with protracted cycling intervals between small stepwise increases in ΔK level. The result, a plateau of relatively constant, ΔK-independent, crack growth rate is similar to that observed by Scott and Sylvester [3].

IV. MICRO LIGAMENT CREEP/CORROSION MODELING OF DATA

Earlier NRL work provides a way of correlating crack-growth-rate data with cyclic plus monotonic stress-strain properties. Details of this procedure may be found in references [11] and [12], the latter of which contains the derived growth rate curve family for this A-36 steel. Briefly, the model views crack growth as a means of straining (hence strain-hardening) material within a fracture process zone at the crack tip. The total amount of strain-hardening which is required derives from two separated sources. The primary source is viewed as the stress relaxation, a consequence of a materials strain-rate sensitivity. At given temperature, it is independent of environment. The secondary source, the

6

environmental effect, is modeled as a bit of surface attack in the cycle which has the effect of surface removal, hence strength reduction via reduction in area.

The amount of surface attack in one cycle is again subdivided. The primary limit, as in ordinary corrosion processes, is time or cycle duration. Its secondary limit, after time is ample, is surface saturation with reacted species. Once this has occurred, generation of the ratelimiting process is paced by the rate amount of clean surface area, plastic deformation, and corresponding dislocation/disruption at the surface, due to crack loading in each cycle.

In this model the mode of strain hardening is also separately assigned: cyclic strain hardening is assumed to counteract creep; monotonic hardning to effects of surface attack. A stress ratio effect derives from associating the cyclic strain hardening with the strain excursion vs monotnic hardening with maximum strain, both augmented by a slight, but simple and deterministic, crack closure correction.

Too complex for manual calculation, the measured stress-strain data is computer-processed to provide parametric maps of possible crack growth paths. Figs. 14 and 15 show these for the two stress ratios utilized: $R = 0$ and 0.8 respectively. The curves are indexed to denote the kind and amount of surface attack. Capital N values pertain to time-limited surface attack where 2^N is that amount, a linear depth of surface annihilation, relative to the radius of the process zone ligament $(d_T/2)$. Capital M is the power of two for plastic-strain-limited surface attack. The matching of the parametric crack growth path maps the fatigue crack growth rate, FCGR, to data plots is restricted to relative translation along the diagonal lines drawn on each. The relative position at match fixed the process zone size, in this case $d_T = 80 \, \mu m$, a value typical of low-medium strength steel [11].

Two ways of fitting the $R = 0$ data are suggested: first, conceding the absence of a stage two transition in the 0.3 and 0.1 Hz data; and secondly, attempting to discern such a transition. Forgoing a transition, frequency independent curve members $M = -1$ and $M = -3$ fairly well fit the lower and high-frequency trends respectively at $d_T = 80 \, \mu m$. In the threshold region a constant N, or fixed

amount of surface attack curve is applicable. That of value $N = -17$ is shown, but this value is judged more from the $R = 0.8$ data. The overlay of these lines on the $R = 0$ data of Fig. 12 is shown in Fig. 16.

The struggle to perceive a transition is shown in Fig. 17. Here a stage one growth for the lower frequencies sea water data is tracked by an $M = -0.5$ curve; a stage two transition by $N_{II} = 11$, and stage three by $M_{III} = -2$. Here the air data is taken to form a population of somewhat reduced growth rate, lying with lower limit along the G_2 line of nil environmental effect. Values of these fitting parameters are generally consistant with those found for FCGR data on other mild steels [12]. However, the fit leaves much to be improved, hence the existance of a stage two transition cannot be assered with any certainty.

Regarding now the high stress ratio data, Fig. 18 shows the growth path curve of $N_{III} = -17$ overlaid from Fig. 15. The flat behavior in this region is associated with the rather active yield point behavior in monotonic loading. In this ΔK range, only monotonic properties govern as only the maximum strain, and not the cyclic strain range, exceeds the proportional limit of the material. The growth here in this modeling algorithm is identified with a threshold level of fixed frequency-independent environmental attack. The value of this threshold, $N_{III} = -17$ is consistant with values of N found in modeling the data of Scott and Sylvester [12]. The model prediction of threshold at high stress ratio is largely dependent on a crack closure correction. The rather crude correction presently employed lacks accuracy and needs improvement. However, the general tendency for growth rate to flatten out to a constant rate in approach to the threshold of growth, a characteristic of this modeling, has been observed in a number of steels [12].

V. DISCUSSION

Present results indicate that the relatively low yield strength of A36 steel has not conferred an exceptional immunity from accelerated failure rate in the at-sea environment. For given crack size and

8

loading, cracks will grow as rapidly as in higher strength structural steels. The problem is less severe only because its allowable static stresses, and correspondingly the K-excursion for a given flaw size are lower.

The failure to verify a stage-two limit to the crack growth rate in salt water is perplexing. A few possible reasons were noted earlier. From a practical viewpoint, a structural reliability assessment assuming no stage-two limit would tend to be conservative, though not greatly so. The crack propagation life of most structures is little affected by the upper regions of the crack growth rate curve; most of the life is expended at very low growth rates near the threshold of the small crack regime.

VI. CONCLUSIONS

From this study of fatigue crack growth rate in A36/A283 structural steel, in air and freely corroding in still sea water, applying extremes of positive stress ratio and varied cyclic frequency, it may be concluded that:

1 . The crack growth rate behavior in air is similar to that of these structural steels in a range of strengths up to twice that of A36.

2. The crack growth in sea water for cycle durations equal to or less than one second is about the same as in air.

3. For longer cycle duration in salt water, the mid-range of crack growth rate exhibits an acceleration of about a factor of three.

4. The crack growth acceleration shows little evidence of limitation by a frequency dependent stage two growth regime.

5. The softer condition of A36 relative to higher strength structural steels does not appear to confer any special immunity from large, detrimental effects of sea water immerson on crack growth rate, hence fatigue endurance of structural components fabricated from it.

9

ACKNOWLEDGMENTS

REFERENCES

1. O. Vosikovsky, "Fatigue Crack Growth In An X-65 Line Pipe Steel At Low Cyclic Frequencies in Aqueous Environments," Trans. ASME, J. Eng. Materials and Technology, Vol. 97, 1975 pp. 298-304.

2. Stress Corrosion Cracking in High-Strength Steels and In Titanium and Aluminum Alloys, B. F. Brown, Editor, Report of ARPA Project 878, U. S. Government Printing Office, Washington, D. C. 1972.

3. P. M. Scott and D.R.V. Sylvester, "The Influence of Mean Tensile Stress on Corrosion Fatigue Crack Growth in Structural Steel Immersed in Sea Water," AERE Harewell, UKOSRP Report 3/02, May 1977.

4. W. H. Bamford, "Application of Corrosion Fatigue Crack Growth Rate Data to Integrity Analysis of Nuclear Reactor Vessels," J. Engineering Materials and Technology, 101, (1979), pp. 182-190.

5. F. V. Lawrence, R. J. Mattos. Y. Higashida, and J. D. Burk, "Estimating the Fatigue Crack Initiation Life of Welds," Fatigue Testing of Weldments, ASTM STP 648, D. W. Hoeppner, Ed., American Society for Testing and Materials, 1978, pp. 134-158.

6. T. R. Gurney, Fatigue of Welded Structures, Cambridge University Press, Cambridge, UK, 1968.

7. Tentative Test Method for Constant-Amplitude Fatigue Crack Growth Rates Above 10^{-8} m/cycle, Test Method #647-78T, Annual Book of ASTM Standards, Part 10, 1980.

8.   A. M. Sullivan and T. W. Crooker, "A Crack-Opening Displacement Technique for Crack Length Measurement in Fatigue Crack Growth Rate Testing - Development and Evaluation," Engineering Fracture Mechanics, 9, (1977), pp. 159-166.

9.   W. H. Cullen, B. H. Menke, H. E. Watson and F. J. Loss, "A Computerized Data Acquisition System for High-Temperature, Pressurized Water, Fatigue Test Facility," Computer Automation of Materials Testing, ASTM STP 710, B. C. Wons'ewicz, Ed., American Society for Testing and Materials, 1980, pp. 127-140.

10. A. M. Sullivan and T. W. Crooker, "Fatigue Crack Growth in A516-60 Steel - Effects of Specimen Thickness, Saline Environment and Electrochemical Potential, Proc. Intnl. Conf. in Fracture Mechanics and Technology, Hongkong, G. C. Sih and C. L. Chow, Eds., Sijthoff and Noordhoff, 1977, pp. 692-697.

11. J. M. Krafft and W. H. Cullen, Jr., "Organizational Scheme for Corrosion-Fatigue Crack Propagation." Engineering Fracture Mechanics, Vol. 10, 1979, pp. 609-650. See also NRL Memorandum Report 3505, July 1977.

12. J. M. Krafft, "Case Studies of Fatigue Crack Growth Using An Improved Micro-Ligament Instability Model," NRL Memo Report 4161, January 1980.
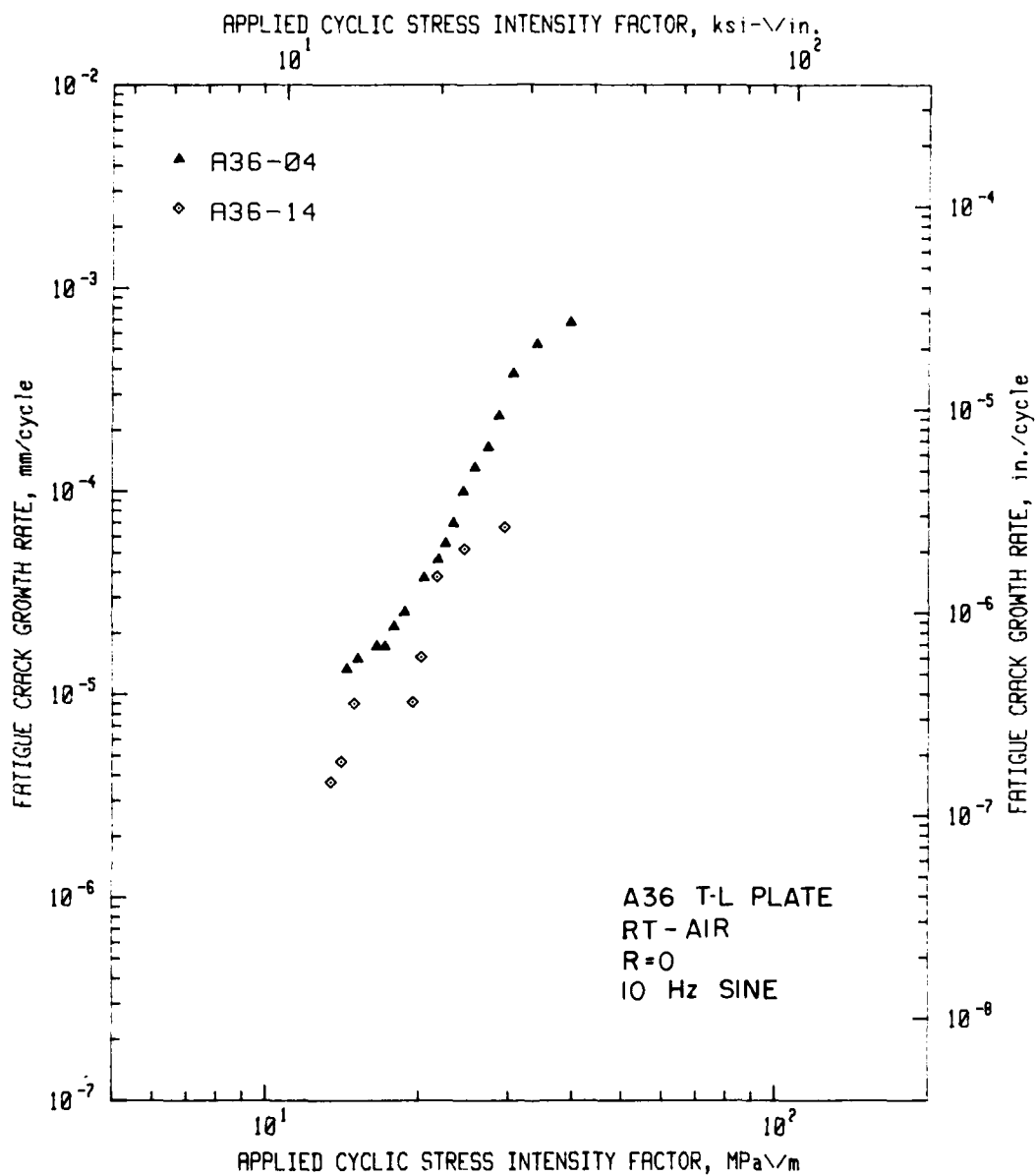
Fig. 1 - Fatigue crack growth rate vs stress intensity factor excursion for A-36 steel plate in air environment, R = 0, loading frequency 10 Hz.
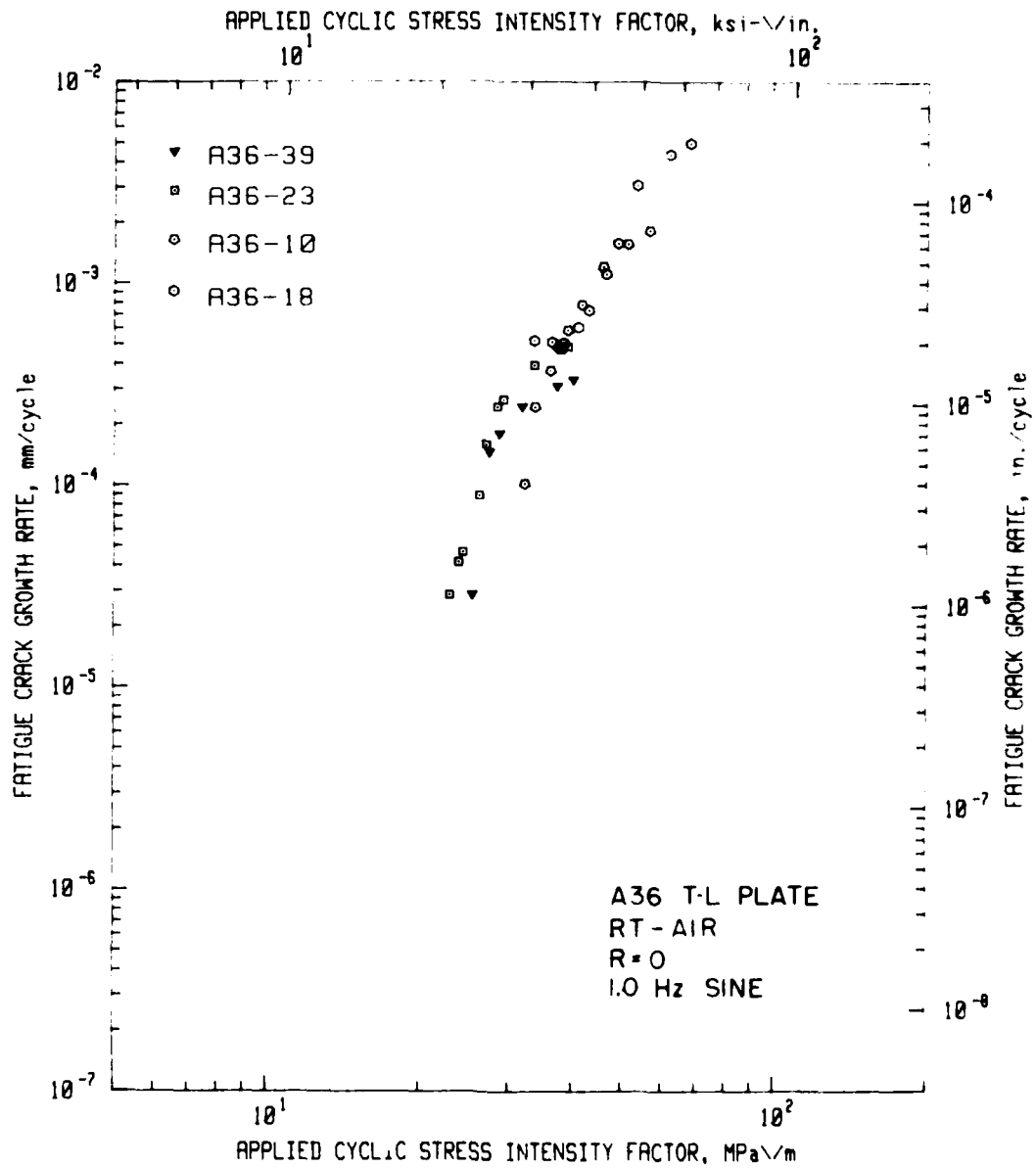
Fig. 2 - As for Fig. 1, but with frequency of 1.0 Hz
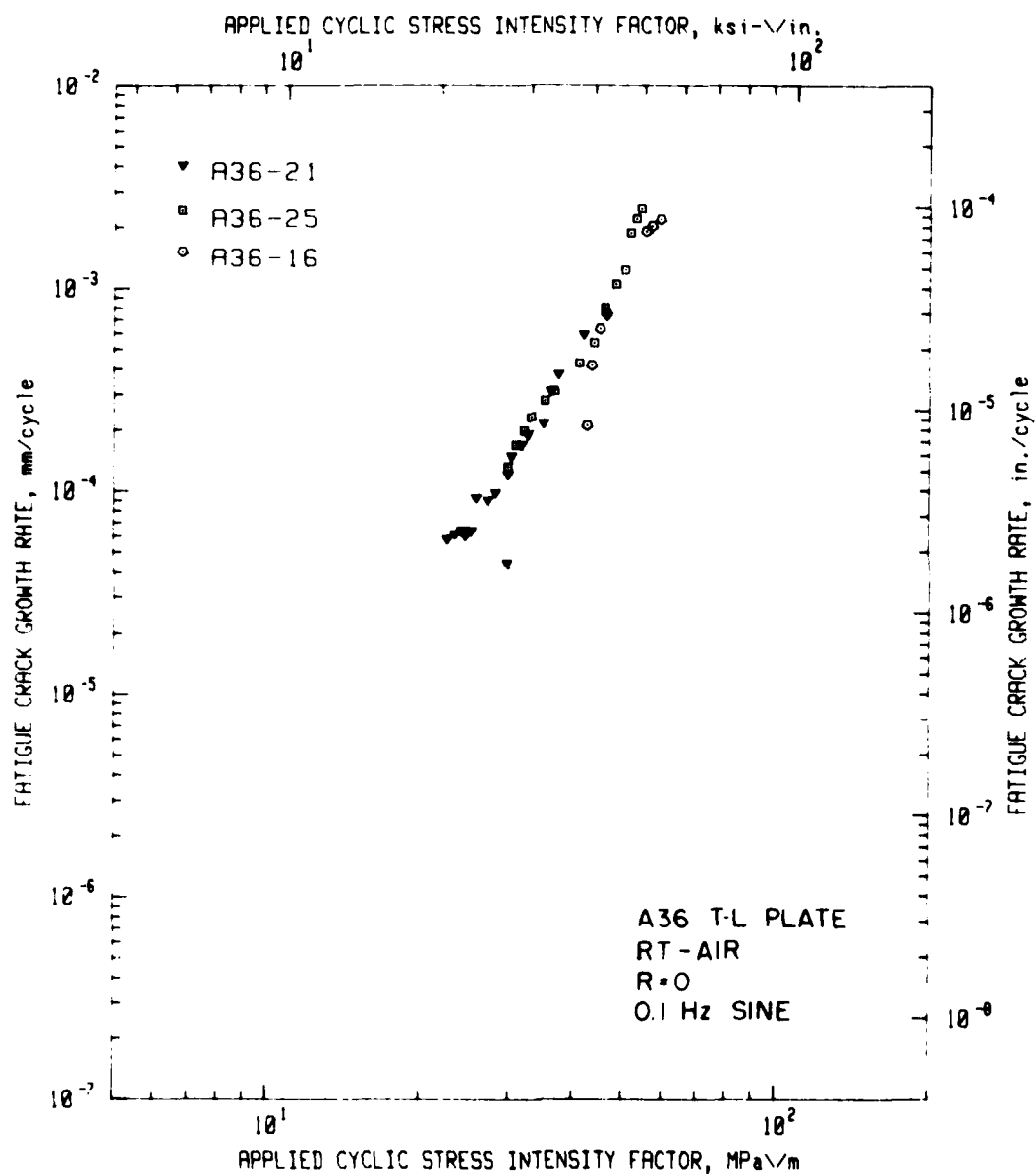
Fig. 3 - As for Fig. 1, but with frequency of 0.1 Hz
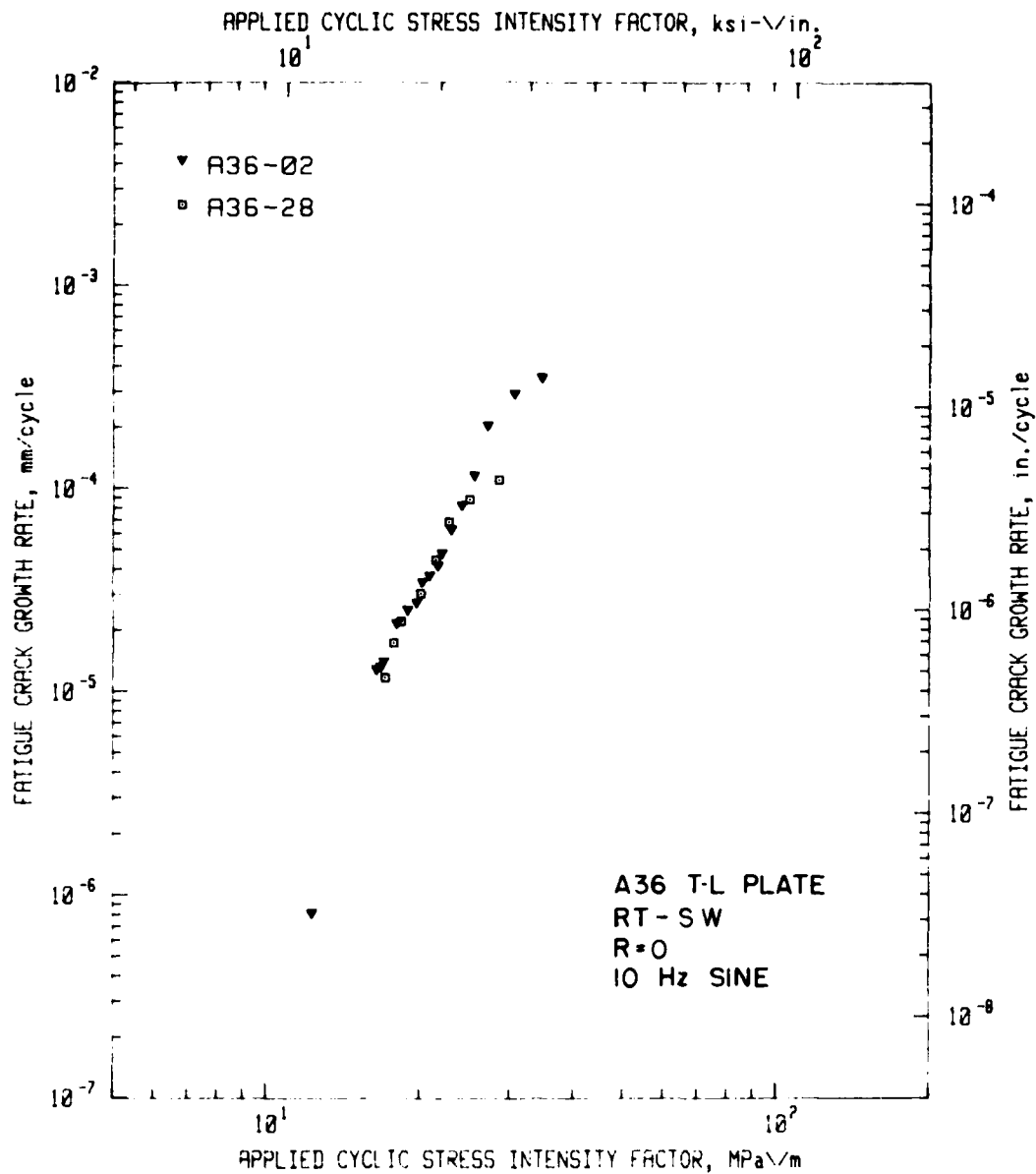
Fig. 4 - Fatigue crack growth rate vs stress intensity factor excursion for A36 steel plate in synthetic sea water environment, R = 0, loading frequency 10 Hz.
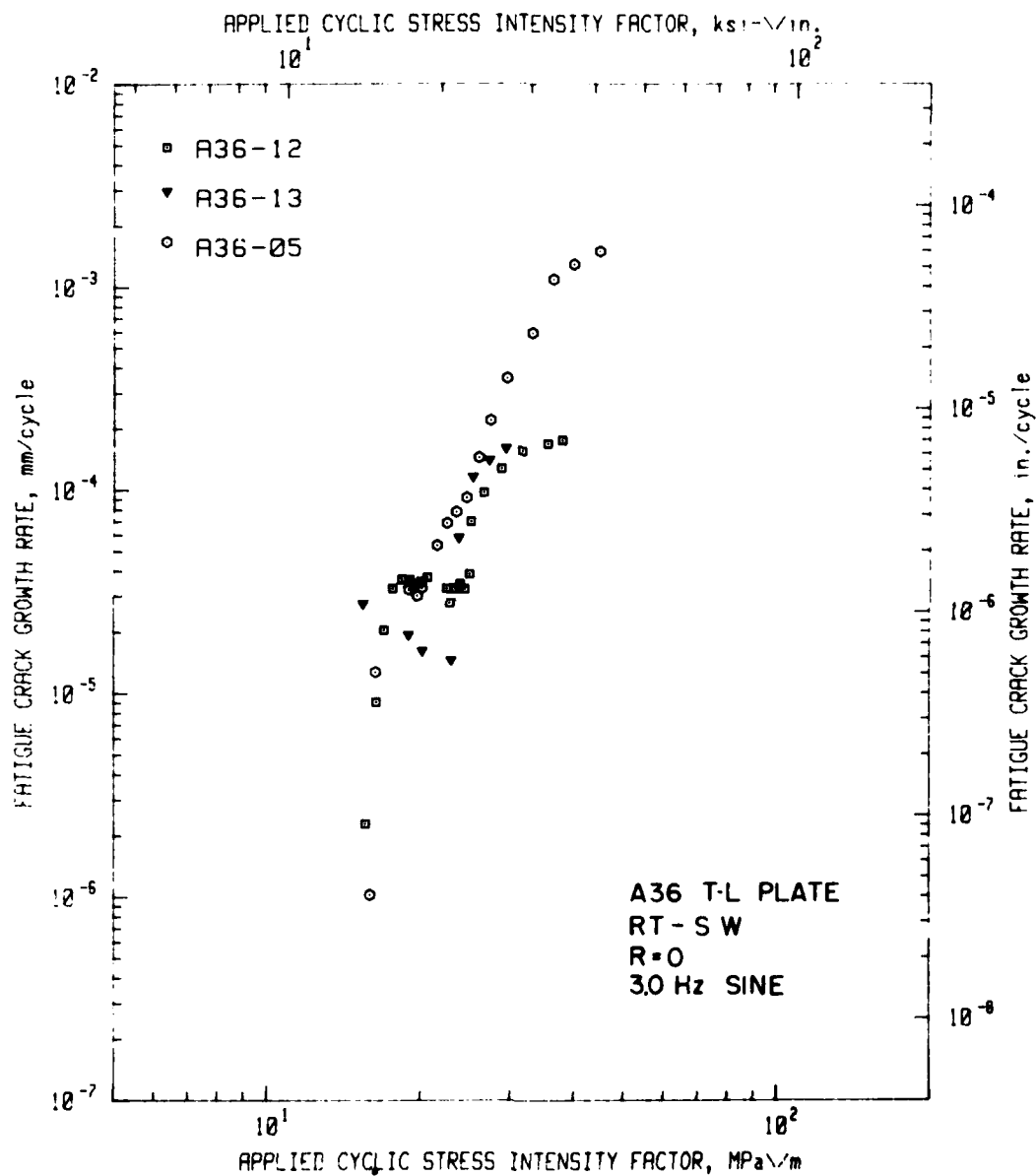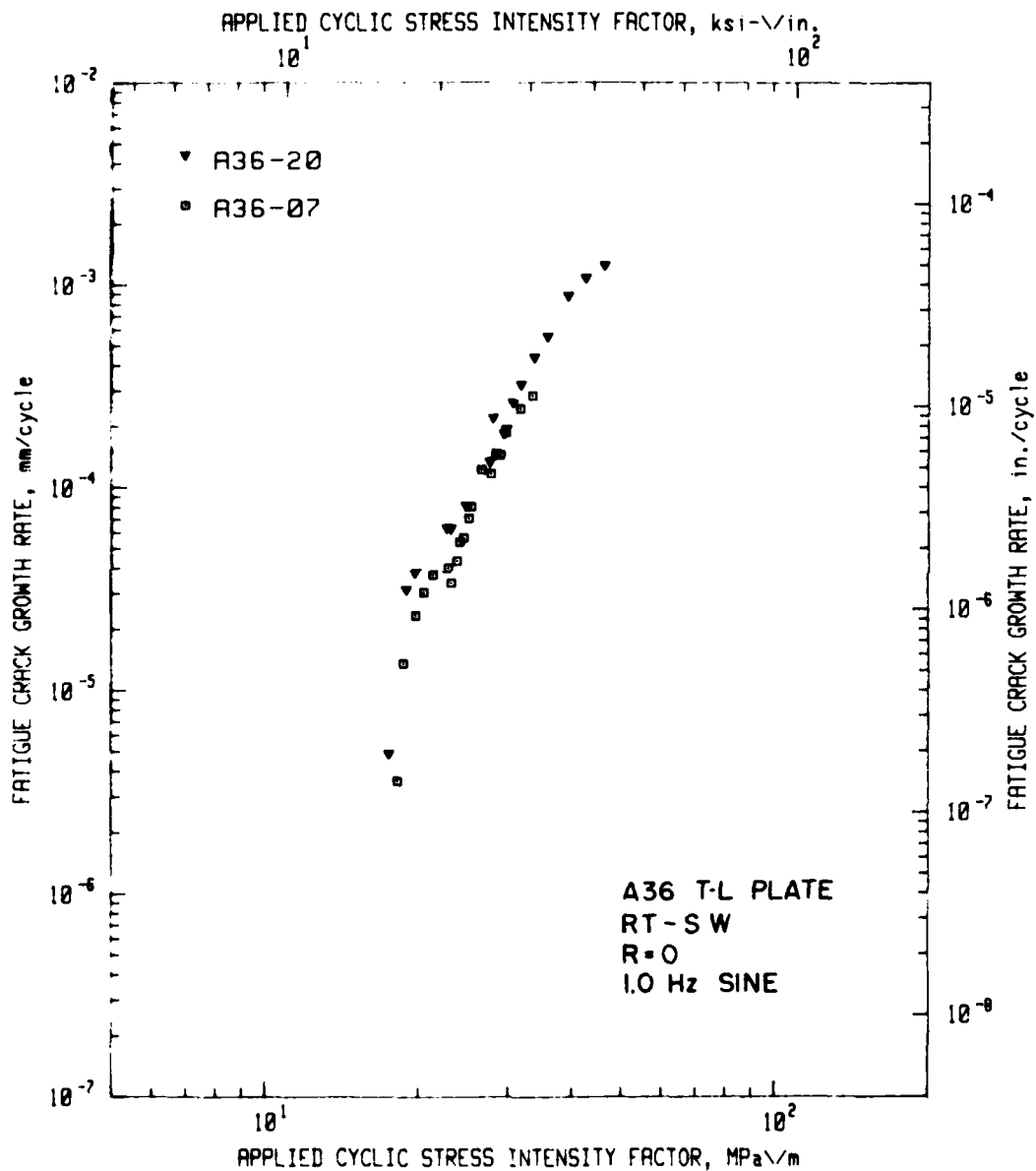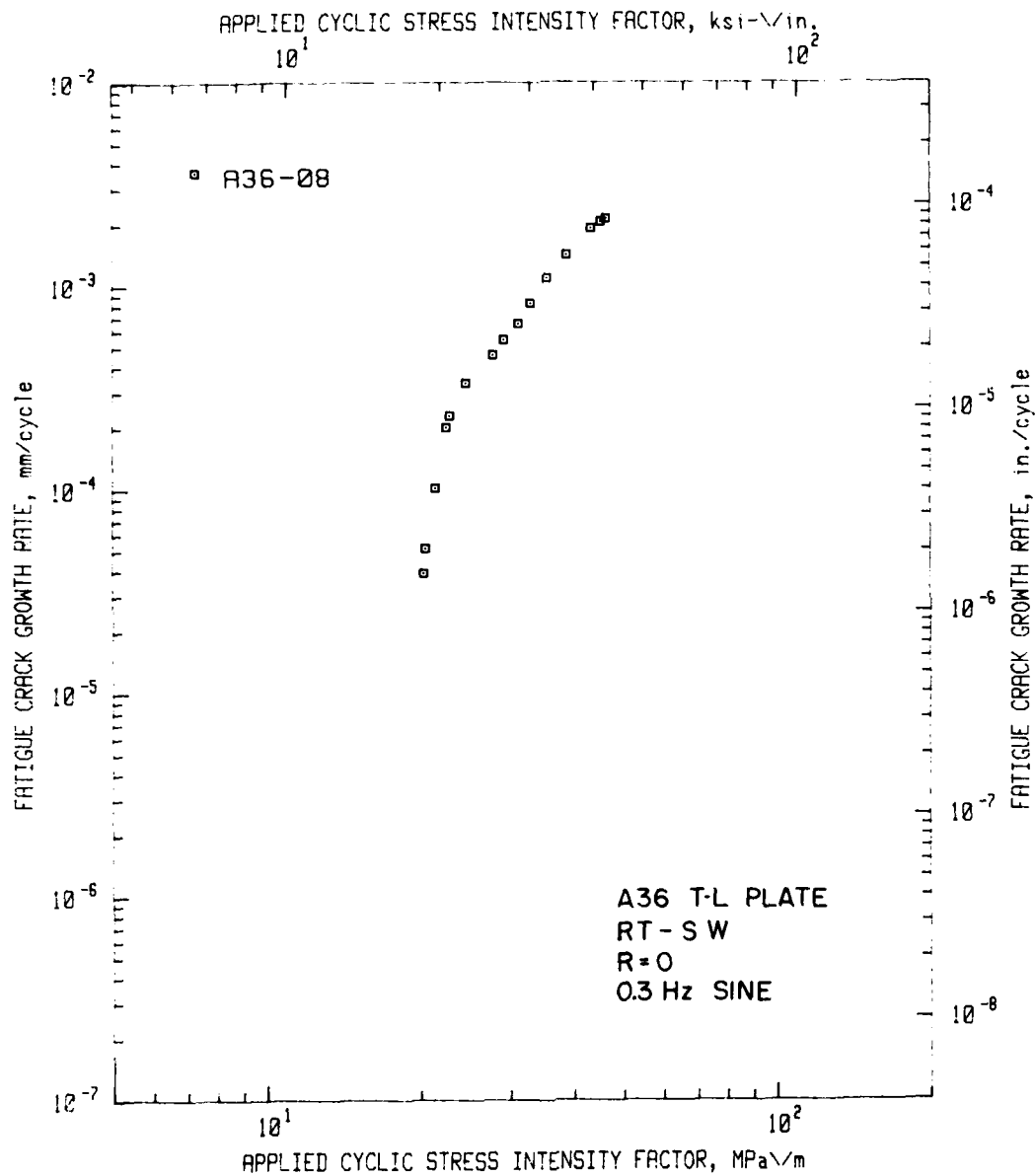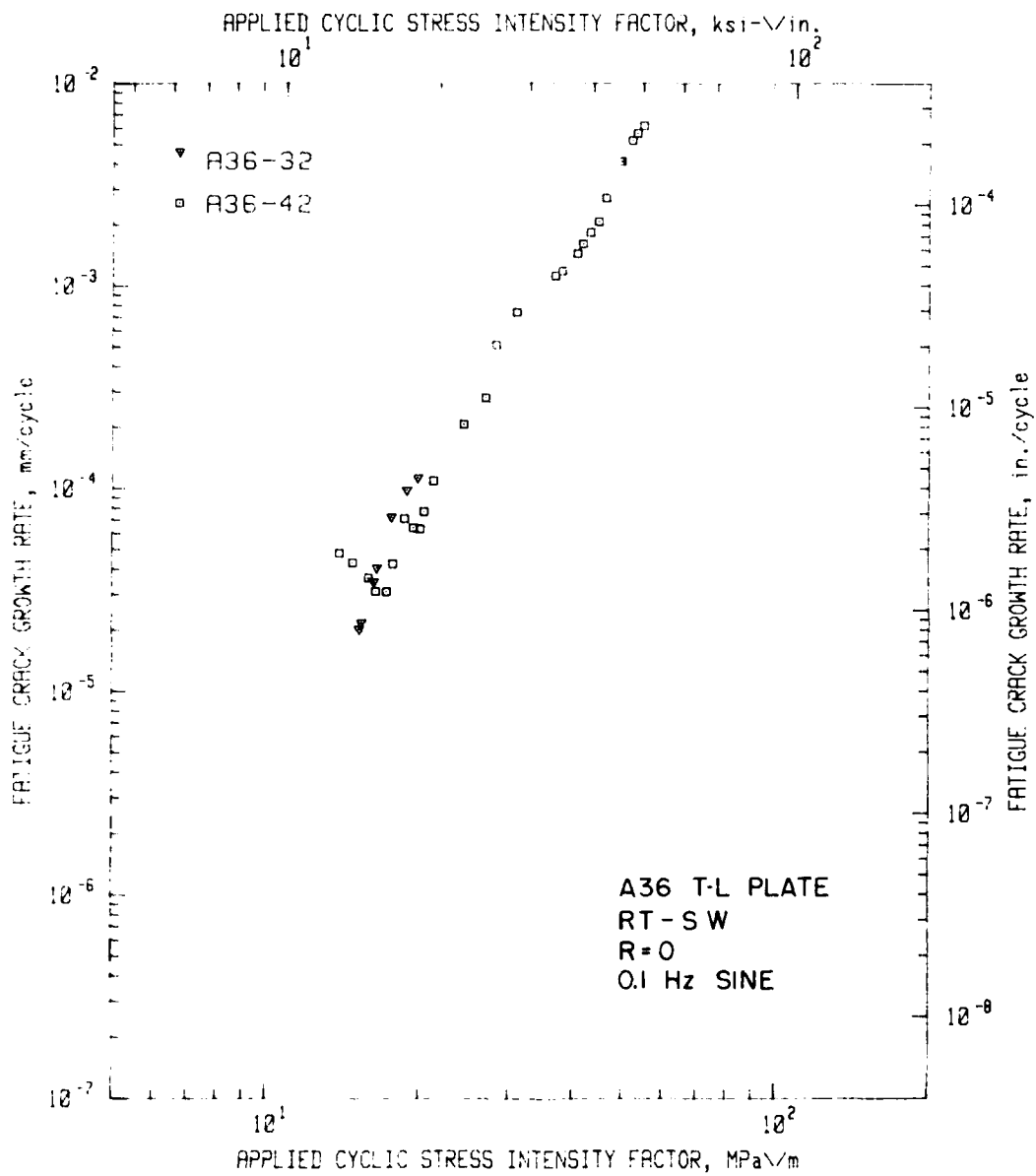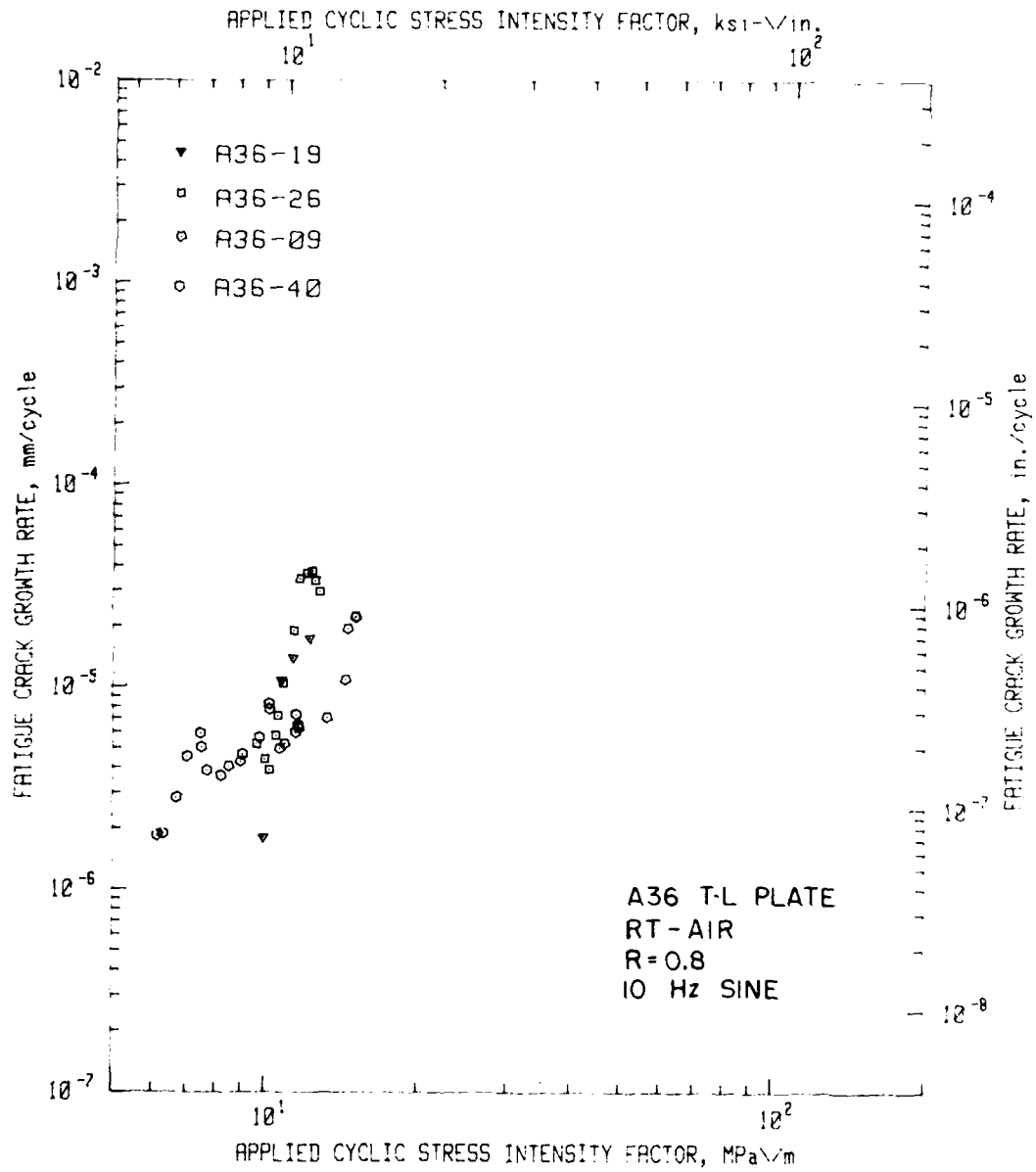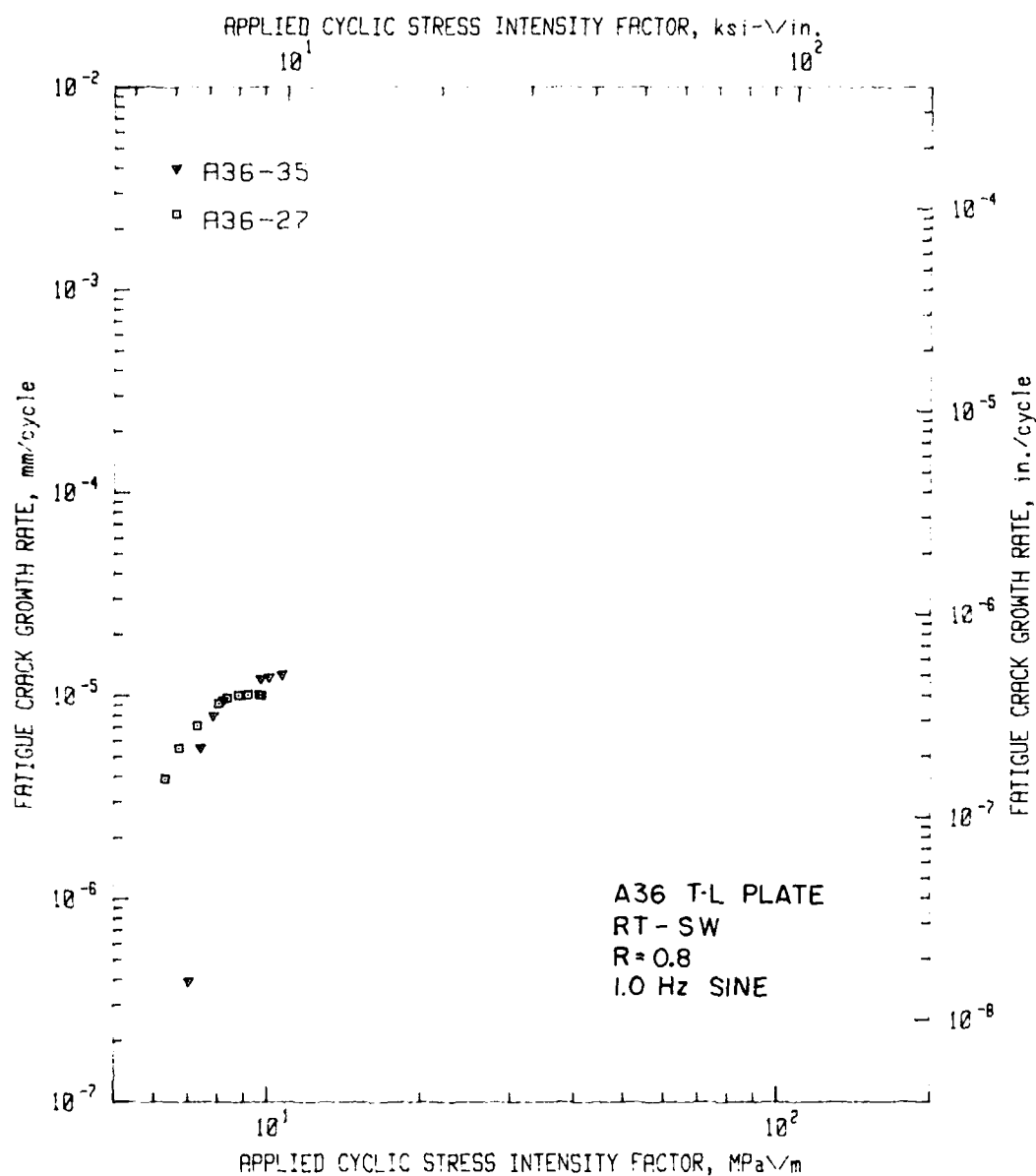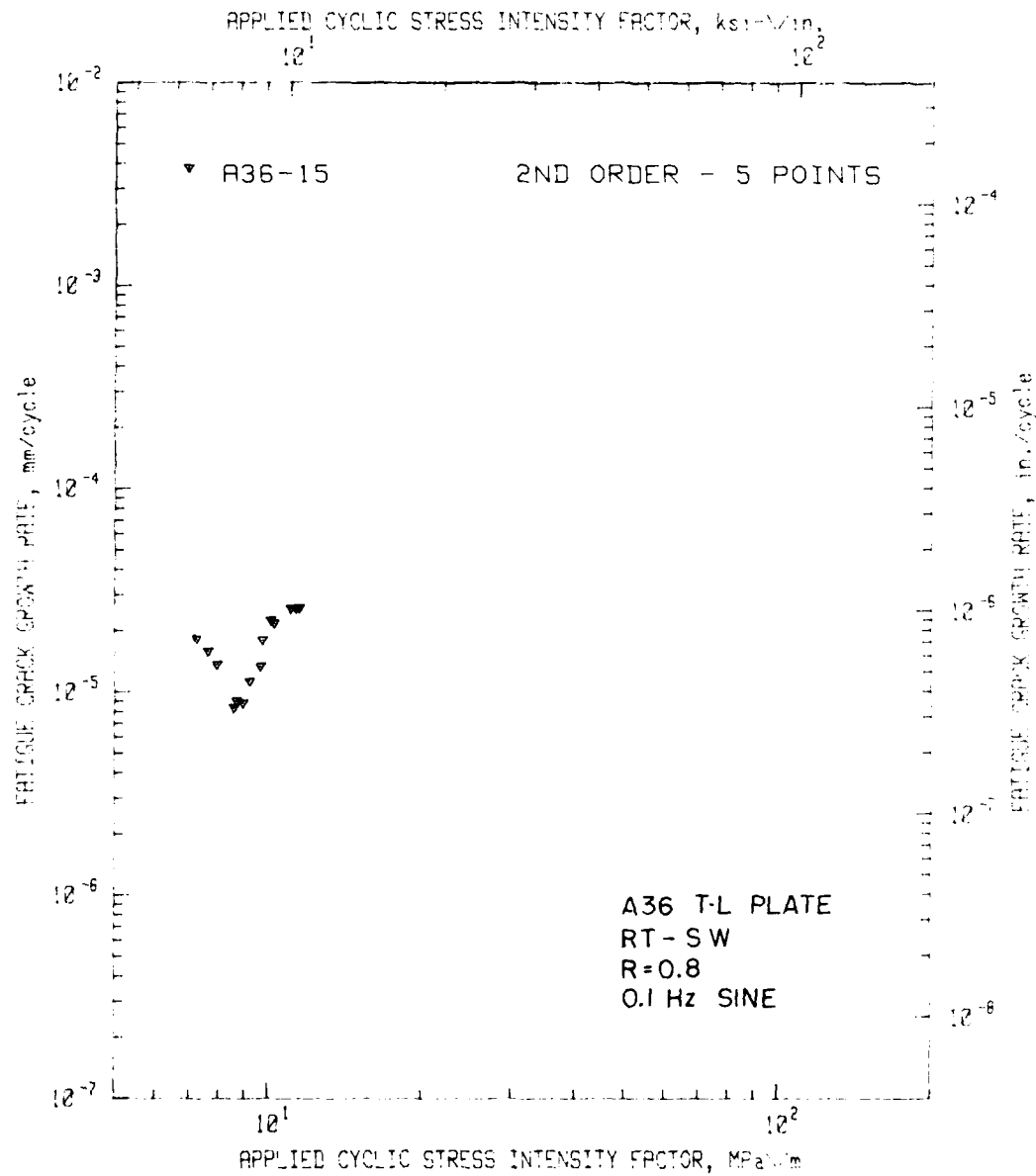
Fig. 5 - As for Fig. 4, but with frequency of 3 Hz

Fig. 6 - As for Fig. 4, but with frequency of 1 Hz.

17

APPLIED CYCLIC STRESS INTENSITY FACTOR, ksi-√in.

A36-08

A36 T-L PLATE
RT - S W
R = O
0.3 Hz SINE

FATIGUE CRACK GROWTH RATE, mm/cycle

FATIGUE CRACK GROWTH RATE, in./cycle

APPLIED CYCLIC STRESS INTENSITY FACTOR, MPa√m

Fig. 7 - As for Fig. 4, but with frequency of 0.3 Hz.

18

APPLIED CYCLIC STRESS INTENSITY FACTOR, ksı-√in.

A36-32

A36-42

A36 T-L PLATE
RT-S W
R=0
0.1 Hz SINE

APPLIED CYCLIC STRESS INTENSITY FACTOR, MPa√m

Fig. 8 - As for Fig. 4, but with frequency of 0.1 Hz.

Fig. 9 - Fatigue crack growth rate vs stress intensity factor excursion for A36 steel plate in air, R = 0.8, loading frequency 10 Hz.

20

Fig. 10 - Fatigue crack growth rate vs stress intensity factor excursion for A36 steel plate in synthetic sea water, R = 0.8, loading frequency 1.0 Hz.

Fig. 11 - As for Fig. 10, but with frequency of 0.1 Hz.

APPLIED CYCLIC STRESS INTENSITY FACTOR, ksi-√in.
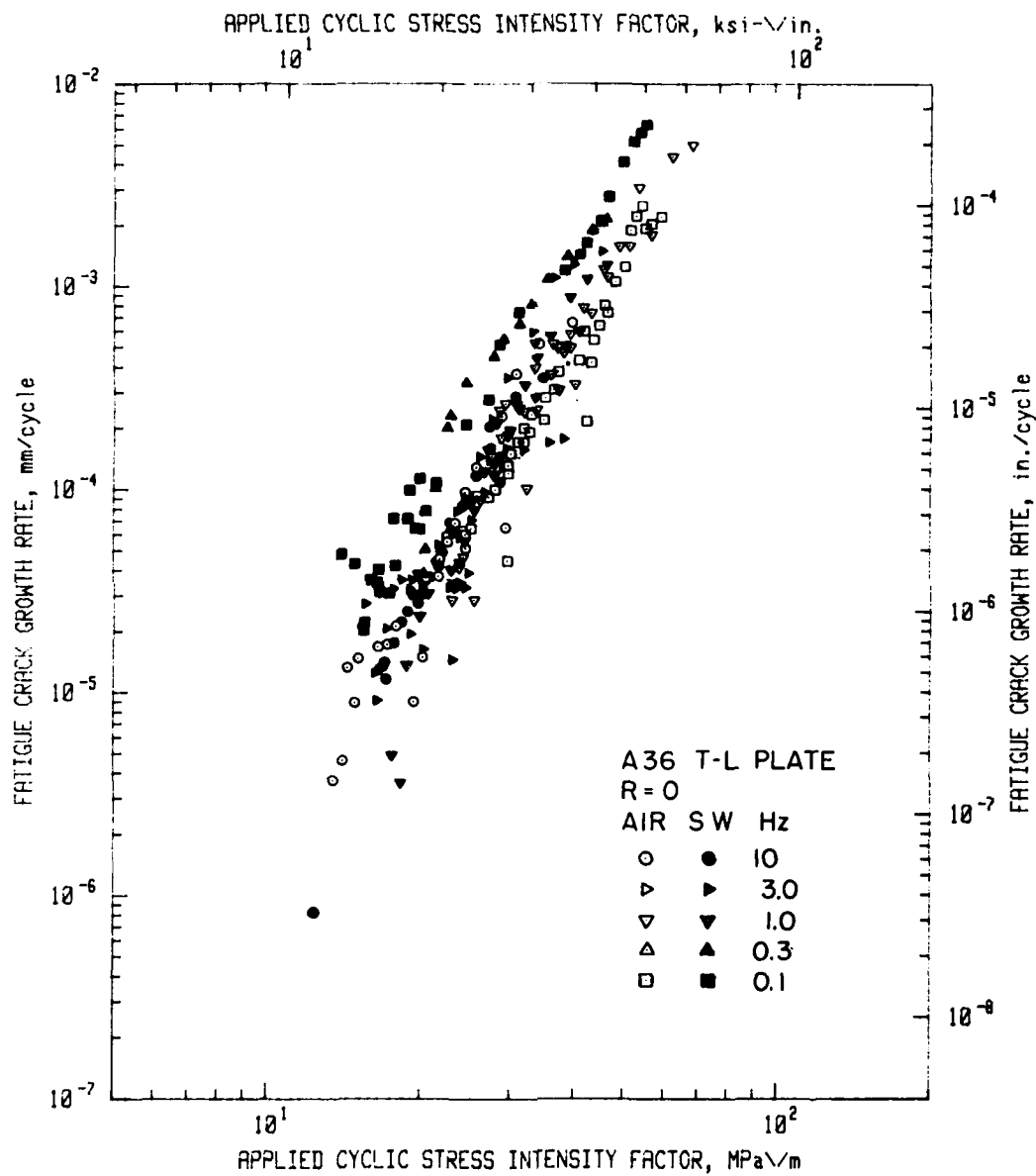
Fig. 12 - Composite plot of all data, with R = 0, Figs. 1-8, both air and
sea water environments and all frequencies.
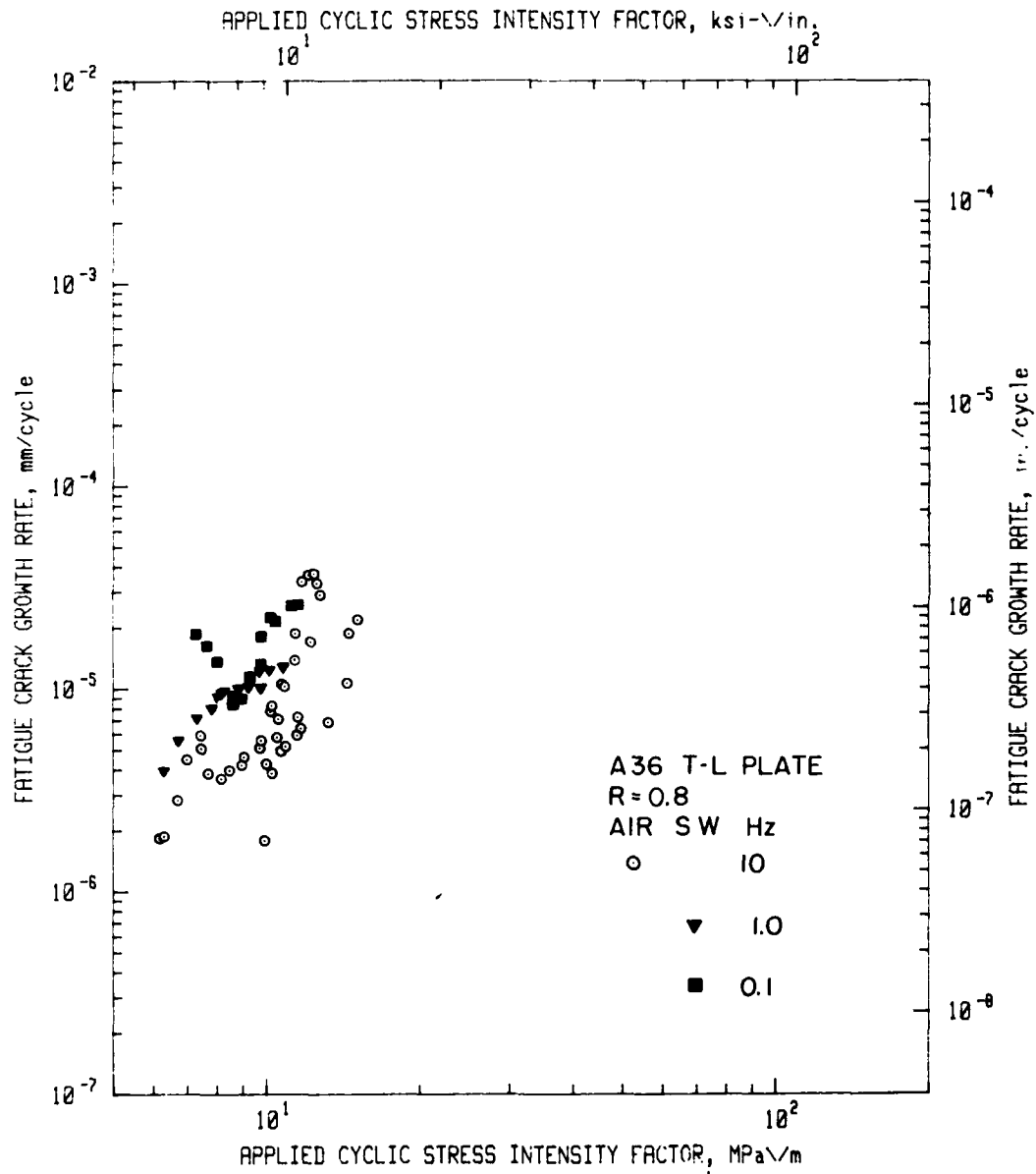
Fig. 13 - Composite plot of all data with R = 0.8. Figs. 9-11, both air and
sea water environments and all frequencies.
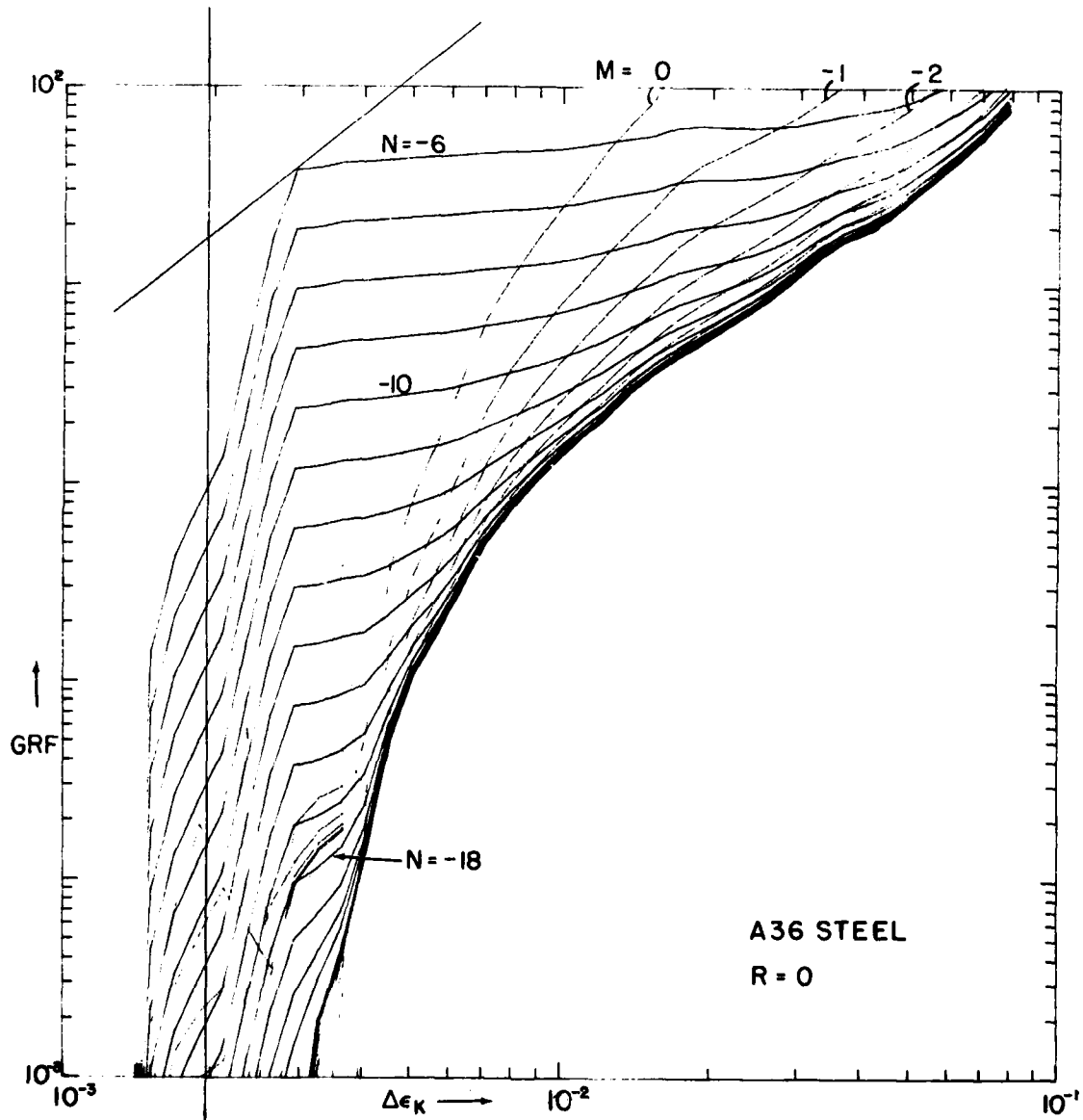
Fig. 14 - Parametric crack-growth-rate-path curves derived from stress strain curves
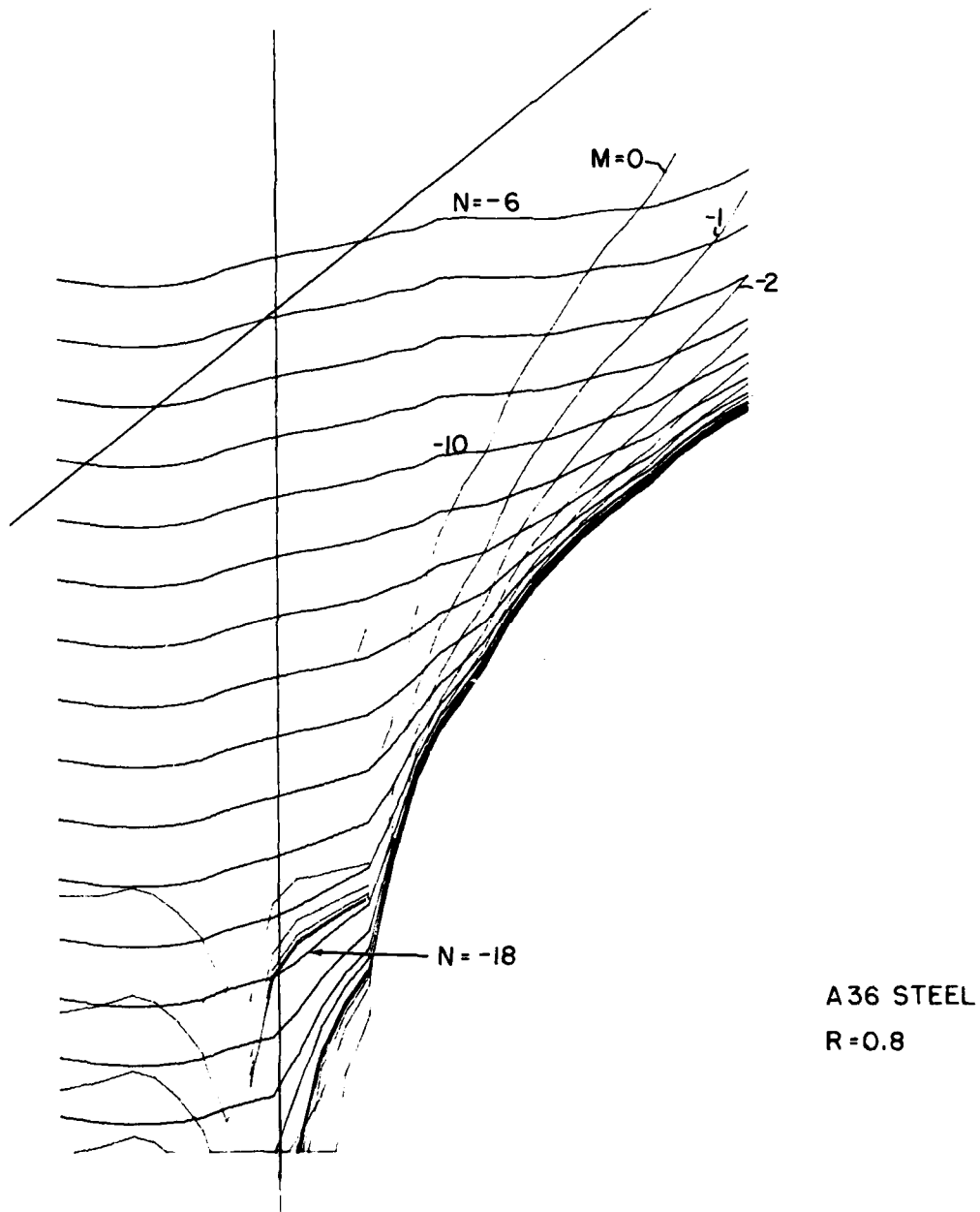of the A36 steel, run for R = 0.

Fig. 15 - As for Fig. 14, but for R = 0.8. Scale, not shown, same as for Fig. 14, may be located from matching line traces of upper left region.

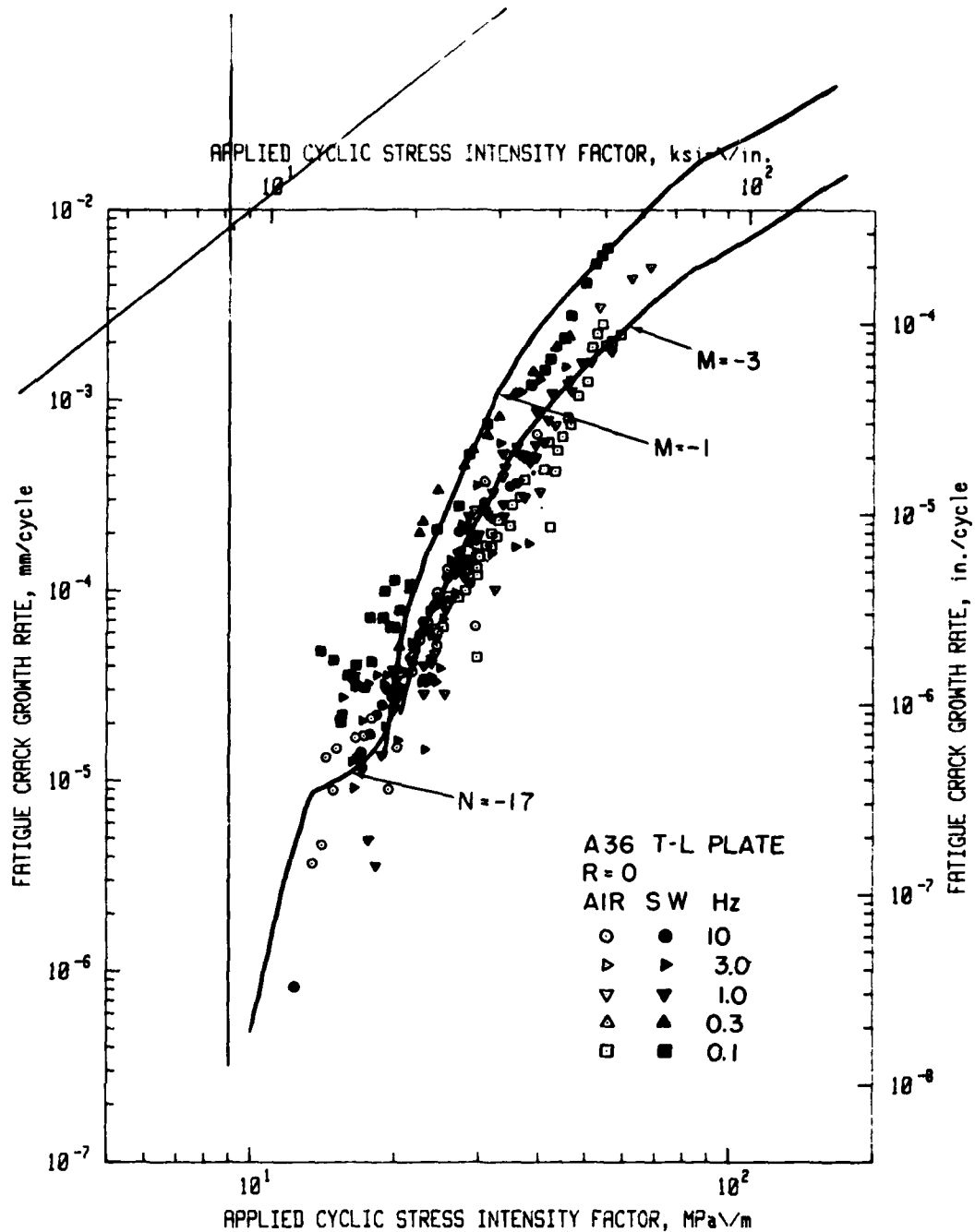Fig. 16 - Parametric curves from Fig. 13 are shown overlaid, the data for R = 0 of Fig. 12. Those selected neglect any possible stage two transition.
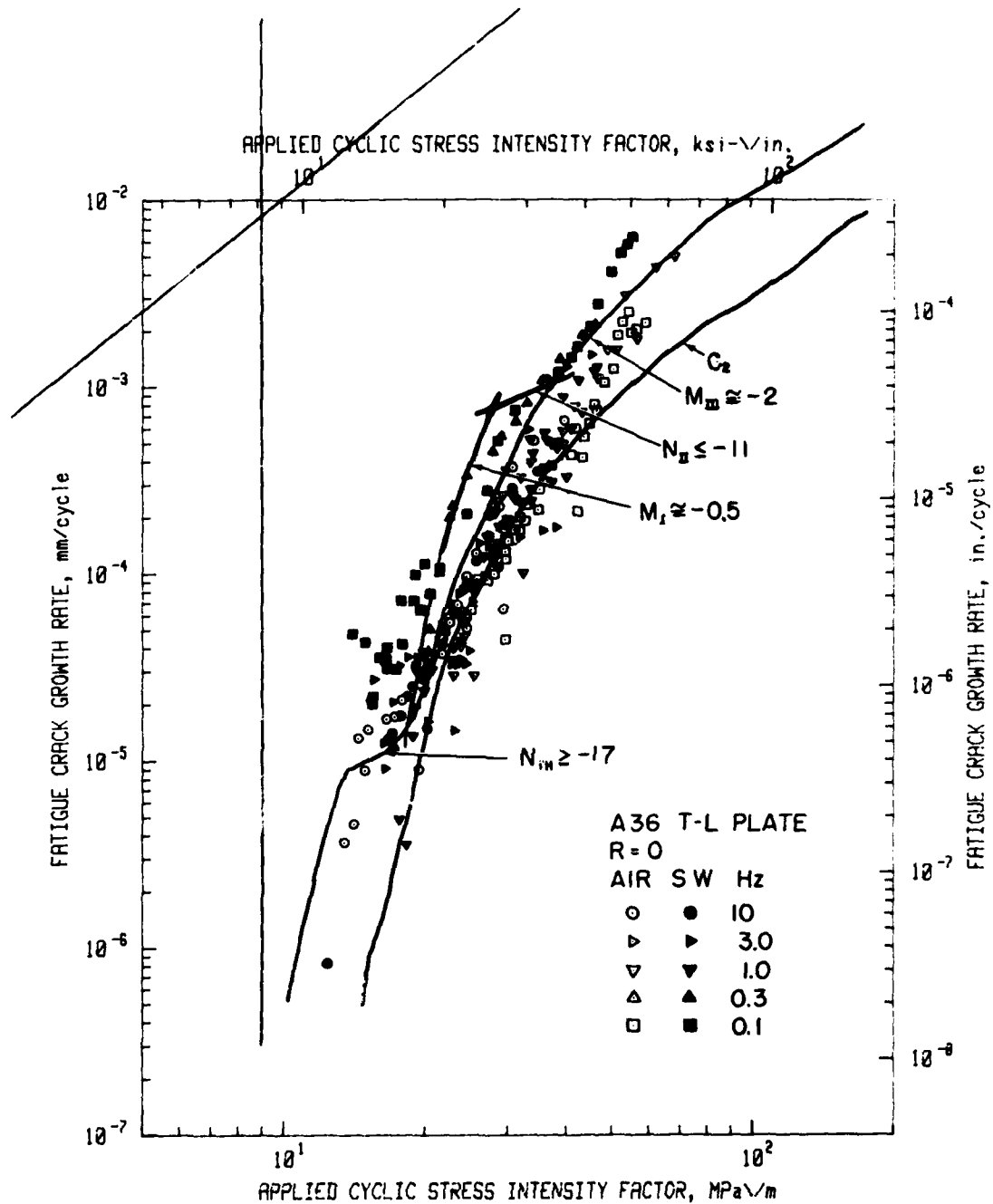
27

Fig. 17 - As in Fig. 16 but with a curve selection suggestive of a possible stage
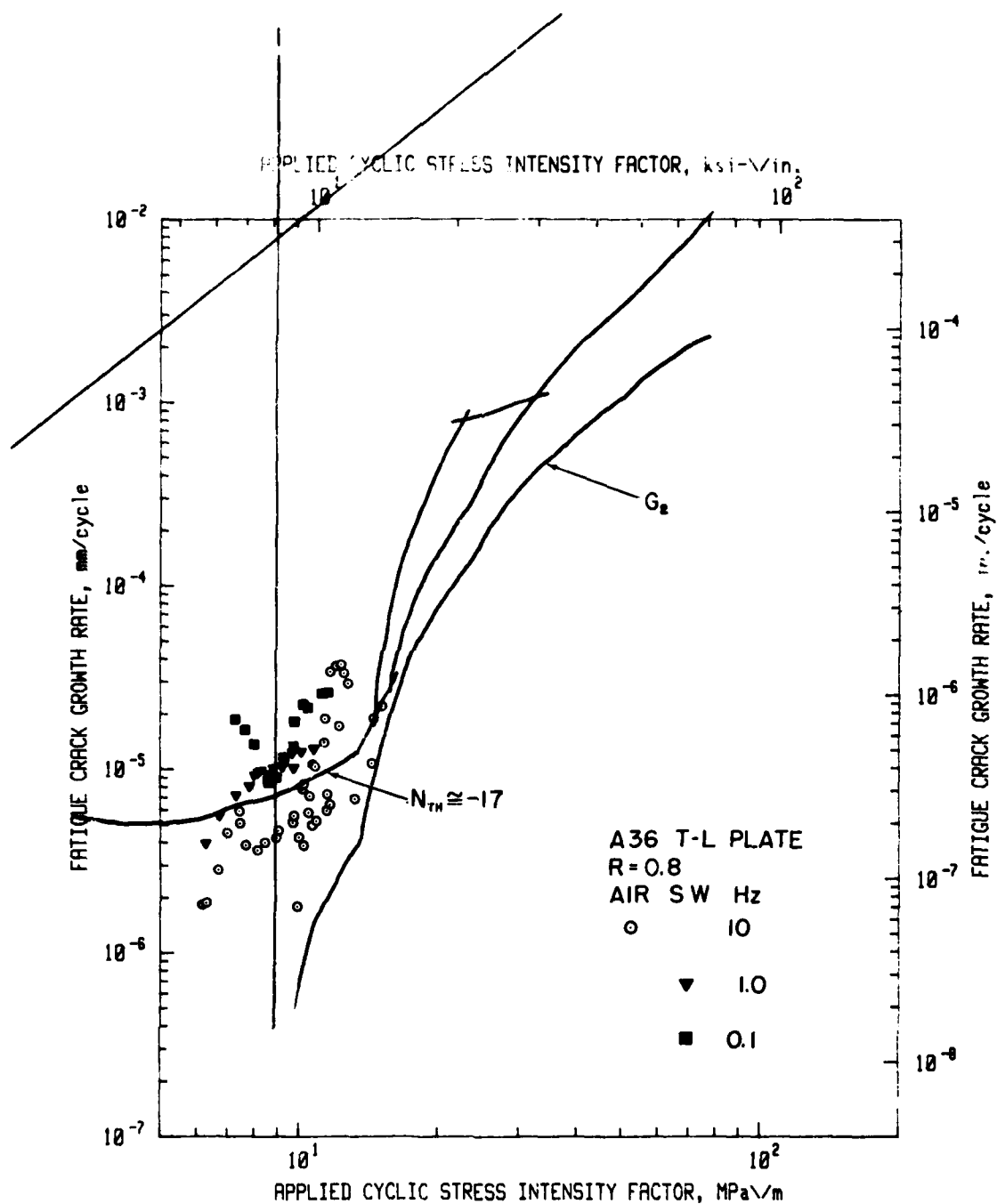two crack growth rate transition.

Fig. 18 - Parametric curves from Fig. 14, are shown in match at $d_T = 8.Fig. 13. \mu m$ to composite data for R = 0.8, Fig. 13. The "constant N" curve members in the threshold region are of same indexes as for the R = 0 data of Figs. 16 and 17.